Low-loss VIS/IR-XUV beam splitter for high-power applications

Ioachim Pupeza,* Ernst E. Fill, and Ferenc Krausz

Max-Planck-Institut für Quantenoptik,
Hans-Kopfermann-Str. 1, 85748 Garching, Germany

*ioachim.pupeza@mpq.mpg.de

Abstract: We present a low-loss VIS/IR-XUV beam splitter, suitable for high-power operation. The spatial separation of the VIS/IR and XUV components of a beam is achieved by the wedged top layer of a dielectric multilayer structure, onto which the beam is impinging under Brewster's angle (for VIS/IR). With a fused silica wedge with an angle of 0.5° we achieve a separation angle of 2.2° and an IR reflectivity of 0.9995. Typical XUV reflectivities amount to 0.1-0.2. The novel element is mechanically robust, exhibiting two major advantages over free-standing Brewster plates: (i) a significant improvement of heat conduction and (ii) easier handling, in particular for high-optical-quality fabrication. The beam splitter could be used as an output coupler for intracavity-generated XUV radiation, promising a boost of the power regime of current MHz-HHG experiments. It is also suited for single-pass experiments and as a beam combiner for pump-probe experiments.

OCIS codes: (340.7480) X-rays, soft x-rays, extreme ultraviolet (EUV); (190.2620) Harmonic generation and mixing; (320.7110) Ultrafast nonlinear optics.

References and links

1. D. Attwood, *Soft X-rays and Extreme Ultraviolet Radiation* (Cambridge University Press, 1999).
2. P. Jaegle, *Coherent Sources of XUV Radiation* (Springer, 2006).
3. I. Pupeza, T. Eidam, J. Kaster, B. Bernhardt, J. Rauschenberger, E. E. Fill, Th. Udem, M. F. Kling, J. Limpert, Z. A. Alahmed, A. M. Azzeer, A. Tünnermann, T. W. Hänsch, and F. Krausz, "Power scaling of femtosecond enhancement cavities and high-power applications," Proc. SPIE **7914**, 79141I (2011).
4. C. Gohle, Th. Udem, M. Herrmann, J. Rauschenberger, R. Holzwarth, H. A. Schuessler, F. Krausz, and T. W. Hänsch, "A frequency comb in the extreme ultraviolet," Nature **436**, 234–237 (2005).
5. R. J. Jones, K. D. Moll, M. J. Thorpe, and J. Ye, "Phase-coherent frequency combs in the vacuum ultraviolet via high-harmonic generation inside a femtosecond enhancement cavity," Phys. Rev. Lett. **94**, 193201 (2005).
6. I. Hartl, T. R. Schibli, A. Marcinkevicius, D. C. Yost, D. D. Hudson, M. E. Fermann, and J. Ye, "Cavity-enhanced similariton Yb-fiber laser frequency comb: 3×10^{14} W/cm^2 peak intensity at 136MHz," Opt. Lett. **32**, 2870–2872 (2007).
7. A. Ozawa, J. Rauschenberger, C. Gohle, M. Herrmann, D. R. Walker, V. Pervak, A. Fernandez, R. Graf, A. Apolonski, R. Holzwarth, F. Krausz, T. W. Hänsch, and Th. Udem, "High harmonic frequency combs for high resolution spectroscopy," Phys. Rev. Lett. **100**, 253901 (2008).
8. D. C. Yost, T. R. Schibli, and J. Ye, "Efficient output coupling of intracavity high harmonic generation," Opt. Lett. **33**, 1099–1101 (2008).
9. I. Pupeza, T. Eidam, J. Rauschenberger, B. Bernhardt, A. Ozawa, E. Fill, A. Apolonski, Th. Udem, J. Limpert, Z. A. Alahmed, A. M. Azzeer, A. Tünnermann, T. W. Hänsch, and F. Krausz, "Power scaling of a high repetition rate enhancement cavity," Opt. Lett. **35**, 2052–2054 (2010).
10. J. Kaster, I. Pupeza, T. Eidam, C. Jocher, E. Fill, J. Limpert, R. Holzwarth, B. Bernhardt, T. Udem, T. W. Hänsch, A. Tünnermann, and F. Krausz, "Towards MW average powers in ultrafast high-repetition-rate enhancement cavities," High Intensity Lasers and High Field Phenomena (HILAS) Conference, paper HFB4 (2011).

#146865 - $15.00 USD Received 29 Apr 2011; revised 30 May 2011; accepted 30 May 2011; published 7 Jun 2011

11. T. Eidam, S. Hanf, E. Seise, T. Andersen, V. T. Gabler, C. Wirth, T. Schreiber, J. Limpert, and A. Tünnermann, "Femtosecond fiber CPA system emitting 830 W average output power," Opt. Lett. **35**, 94–96 (2010).
12. P. Rußbüldt, T. Mans, J. Weitenberg, H. D. Hoffmann, and R. Poprawe, "Compact diode-pumped 1.1 kW Yb:YAG Innoslab femtosecond amplifier," Opt. Lett. **35**, 4169–4171 (2010).
13. I. Pupeza, X. Gu, E. Fill, T. Eidam, J. Limpert, A. Tünnermann, F. Krausz, and Th. Udem, "Highly sensitive dispersion measurement of a high-power passive optical resonator using spatial-spectral interferometry," Opt. Express **18**, 26784–26195 (2010).
14. K. D. Moll, R. J. Jones, and J. Ye, "Nonlinear dynamics inside femtosecond enhancement cavities," Opt. Express **13**, 1672–1678 (2005).
15. R. Paschotta, "Beam quality deterioration of lasers caused by intracavity beam distortions," Opt. Express **14**, 6069–6074 (2006).
16. Y.-Y. Yang, F. Sümann, S. Zherebtsov, I. Pupeza, J. Kaster, D. Lehr, H.-J. Fuchs, E.-B. Kley, E. Fill, X.-M. Duan, Z.-S. Zhao, F. Krausz, S. L. Stebbings, and M. F. Kling, "Optimization and characterization of a highly-efficient diffraction nanograting for MHz XUV pulses," Opt. Express **19**, 1955–1962 (2011).
17. K. D. Moll, R. J. Jones, and J. Ye, "Output coupling methods for cavity-based high-harmonic generation," Opt. Express **14**, 8189–8197 (2006).
18. A. Ozawa, A. Vernaleken, W. Schneider, I. Gotlibovych, Th. Udem, and T. W. Hänsch, "Non-collinear high harmonic generation: a promising outcoupling method for cavity-assisted XUV generation," Opt. Express **16**, 6233–6239 (2008).
19. J. Weitenberg, P. Rußbüldt, T. Eidam, and I. Pupeza, "Transverse mode tailoring in a high-finesse femtosecond enhancement cavity," Opt. Express **19**, 9551–9561 (2011).
20. I. Pupeza, J. Weitenberg, P. Rußbüldt, T. Eidam, J. Limpert, E. Fill, Th. Udem, H.-D. Hoffmann, R. Poprawe, A. Tünnermann, and F. Krausz, "Tailored transverse modes in high-finesse femtosecond enhancement cavities," CLEO 2011, Baltimore, paper QMJ7 (2011).
21. E. D. Palik, *Handbook of Optical Constants of Solids* (Academic Press, 1991), Vols. 1,2.
22. G. Tempea, V. Yakovlev, B. Bacovic, F. Krausz, and K. Ferencz, "Tilted-front-interface chirped mirrors," J. Opt. Soc. Am. B **18**, 1747–1750 (2001).
23. G. Steinmeyer, "Brewster-angled chirped mirrors for high-fidelity dispersion compensation and bandwidths exceeding one optical octave," Opt. Express **11**, 2385–2396 (2003).
24. T. Eidam, F. Röser, O. Schmidt, J. Limpert, and A. Tünnermann, "57 W, 27 fs pulses from a fiber laser system using nonlinear compression," Appl. Phys. B **92**, 9–12 (2008).

1. Introduction

Over the past decades, the development of high-power ultrafast laser sources enabled intense research in the field of high-harmonic generation (HHG). Nowadays, for numerous applications in fundamental research, technology and life sciences, involving the generation of broadband extreme ultraviolet (XUV) light [1–3], HHG systems constitute a convenient table-top alternative to synchrotrons. The medium for the highly nonlinear process of HHG is usually a noble gas and intensities on the order of 10^{13} W/cm^2 in the visible and/or infrared range (VIS/IR) are necessary to drive HHG. The conversion efficiency of the fundamental radiation (FR) to the high harmonics (HH) typically lies between 10^{-9} and 10^{-6}, resulting in a significant difference between the power levels of the driving FR and the HH. Moreover, most optical materials exhibit fundamentally different properties in the VIS/IR and XUV ranges. Thus, in the frame of HHG experiments, the design of low-loss optical elements such as beam splitters and combiners is highly challenging.

One of the most prominent state-of-the-art HHG setups, in which this shortcoming plays a major role, relies on the enhancement of high-repetition-rate laser pulses by several orders of magnitude in a high-finesse passive resonator, also called "enhancement cavity" [4–9]. Here, the seeding laser light is interferometrically overlapped with the light circulating inside the cavity. In this manner, energy is continuously coupled to the cavity. In an intracavity focus, the peak intensities for HHG are reached with multi-10-MHz repetition rates. On the one hand, this implies a significant increase of the overall conversion efficiency of the FR to the HH. On the other hand, many applications like frequency comb or coincidence spectroscopy are expected to benefit from the high repetition rates of the intracavity-generated XUV pulses. Recently, the ultrafast MHz-repetition-rate enhancement cavity technology has been scaled up to mJ-

#146865 - $15.00 USD Received 29 Apr 2011; revised 30 May 2011; accepted 30 May 2011; published 7 Jun 2011

level circulating pulse energies [9]. New cavity designs [10] seeded by recently developed, powerful laser sources such as reported in [11, 12] promise further substantial scaling in the near future. However, to this day, one of the main limitations of the circulating power inside an enhancement cavity for HHG is imposed by the XUV output coupling element, i.e. the optics providing the spatial separation of the FR and the collinearly generated HH. To the best of our knowledge, the circulating power inside femtosecond enhancement cavities including an output coupler [4, 5, 7, 8] is significantly smaller than the power level demonstrated in an empty cavity [3, 9].

In this paper we present a low-loss VIS/IR beam splitter suitable for high-power applications. This novel optical element, which we refer to as *wedge-on-mirror output coupler* (WOMOC), is designed to circumvent limitations of current output couplers for intracavity-generated XUV radiation and to enable a boost of the power regime in intracavity HHG. However, the WOMOC might also be employed to separate the XUV from the FR in single-pass HHG systems or to recombine a VIS/IR and an XUV beam collinearly, e.g. for pump-probe experiments.

The manuscript is structured as follows: in Section 2 the design criteria are discussed and current output coupling methods for intracavity HHG are briefly reviewed, in Section 3 the mode of operation of the WOMOC is described, Section 4 reports on the experimental realization and the characterization of the WOMOC and Section 5 concludes the paper.

2. Design criteria and existing XUV output couplers for intracavity HHG

The design criteria discussed in this section are related to the task of coupling out intracavity-generated XUV radiation. However, they are also desirable in the context of single-pass beam splitting and/or combining.

There are two categories of effects limiting the power enhancement of a frequency comb inside a HHG enhancement cavity. Firstly, intracavity losses attenuate the electric field amplitude upon each round trip. These losses are mainly caused by the cavity optics and the interaction with the nonlinear medium employed for HHG. Typical state-of-the art low-loss, low-dispersion, highly reflecting dielectric mirrors for visible/infrared femtosecond pulses exhibit power loss values of around 50 ppm. The interaction with the gas target strongly depends on the parameters of the circulating pulse and of the gas jet. Secondly, in the case of significantly large optical bandwidths, intracavity dispersion affects the circulating electric field and represents an enhancement limitation. On the one hand, the cavity round-trip dispersion leads to a truncation of the optical spectrum coupled to the cavity due to its unevenly spaced resonances in the frequency domain. On the other hand, dispersion also affects the phase of the circulating field. In the high-power case, where nonlinear effects related to the intracavity propagation of the fundamental beam cannot be neglected, both enhancement-limiting mechanisms exhibit intensity-dependent behavior, see e.g. [13, 14]. Consequently, in a high-finesse, high-power enhancement cavity, an output coupling mechanism for intracavity-generated XUV light must satisfy the following conditions:

- **C1**: The XUV output coupling efficiency should be large.
- **C2**: The effects of absorption and dispersion of the FR due to the interaction with the output coupler should be small.
- **C3**: Nonlinear effects in the output coupler caused by the FR should be small.
- **C4**: The heat caused by the interaction of the FR with the output coupler should be efficiently.
- **C5**: Other losses, like scattering due to poor optical quality or depolarization of the FR should be small.

#146865 - $15.00 USD Received 29 Apr 2011; revised 30 May 2011; accepted 30 May 2011; published 7 Jun 2011

In the first demonstrated HHG enhancement cavity experiments the output coupler was a thin plate, transparent for the FR, placed at Brewster's angle in the cavity beam path as the first optical element after the HHG focus [4, 5, 7]. The collinear superposition of the FR and the generated XUV hits the surface of the plate. The p-polarized FR is transmitted through the plate while the XUV radiation, for which the refractive index of the plate material is smaller than 1, experiences total reflection at the surface, is therefore spatially separated from the FR and coupled out of the cavity. Concerning criterion C1, the XUV reflectivity of materials transparent for the FR under Brewster's angle for the FR typically amounts to ∼10%-20% around 60 nm and decreases for shorter wavelengths. In order to meet the criteria C2 and C3, the thickness of the Brewster plate should be chosen as small as possible. However, decreasing the thickness implies two disadvantages. Firstly, in the vacuum environment necessary for XUV light propagation, the decreased thickness leads to a poor conduction of the heat caused by the absorption in the plate, violating condition C4. As a consequence, the plate introduces a phase front distortion in the cavity, which is likely to affect the excited mode [15] and the enhancement behavior, and the heating might lead to the damage of the plate. Secondly, mechanical processing and handling becomes more difficult for thin plates, often limiting the feasibility of such plates or leading to poor optical quality, violating criterion C5.

There have been several approaches to circumvent the limitations of the Brewster plate output coupler. In [8, 16], a nanostructure is written in the top layer of the cavity mirror following the HHG focus. This optical element acts as a highly reflecting mirror for the FR and as a diffraction grating for the generated XUV, thus providing spatial separation of the HH from the FR. The output coupling efficiency is comparable to that of a Brewster plate. However, the harmonics coupled out of the cavity are angularly dispersed. For several applications, this is a substantial disadvantage. Moreover, while this technique offers the prospect of scaling to higher circulating powers, the nanostructure might constitute a limiting factor due to undesired effects, e.g. an increased nonlinearity, see [16]. Other output coupling mechanisms, such as non-collinear HHG and output coupling through an aperture on the optical axis of the resonator, optionally using higher-order modes, are proposed in [17–20]. However, these techniques either violate one of the necessary conditions listed above or complicate the cavity setup significantly. To the best of our knowledge, none of these output coupling methods has been successfully experimentally demonstrated to this day.

In conclusion, despite the limitations discussed above, for collinear output coupling of intracavity-generated XUV light from a high-finesse resonator, the free-standing Brewster plate output coupler remains the most convenient method so far. The novel optical element presented in this manuscript combines the low-loss advantages of a thin Brewster plate output coupler with the heat conduction properties, the robustness and the optical quality of a state-of the-art dielectric multilayer mirror.

3. Description and mode of operation

3.1. The concept of the WOMOC

Figure 1 shows a scheme of the wedge-on-mirror output coupler (WOMOC). It is a dielectric multilayer structure, the top layer of which is wedged at a small angle α. The physical principle employed for the spatial separation of the FR and the HH component of the intracavity laser beam is the same as for the Brewster plate discussed in the previous section. The p-polarized FR beam impinges on the wedge surface under the Brewster angle ϕ_B for the wedge material. The XUV radiation is reflected at the surface of the WOMOC under the angle ϕ_B. The FR penetrates the wedge and propagates towards the next material interface, under an angle of incidence ϕ_i, which is determined by ϕ_B and α. The subsequent dielectric multilayer structure is designed to act as a high reflector for the FR. The reflected portion travels back through the

#146865 - $15.00 USD Received 29 Apr 2011; revised 30 May 2011; accepted 30 May 2011; published 7 Jun 2011

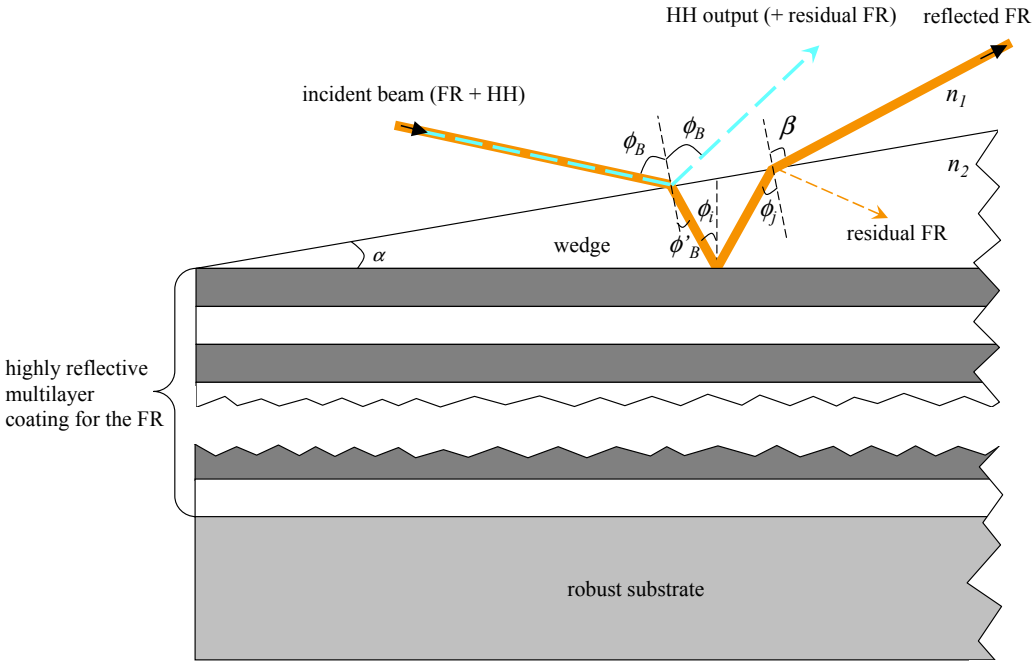

Fig. 1. The WOMOC. FR: fundamental radiation (p-polarized), HH: high harmonics. The multilayer stack underlying the wedge is matched to the adjacent medium n_2 and for the angle of incidence ϕ_i.

wedged layer and hits its surface under an angle ϕ_j. If α and the fundamental beam divergence are small, the deviation of ϕ_j from the Brewster angle for this interface is small, such that (i) the overall losses of the fundamental beam upon reflection at the WOMOC are small and (ii) the fundamental is reflected by the WOMOC under a slightly larger angle $\beta > \phi_B$ than the HH, providing the spatial separation of the two components. In the following, we derive the separation angle between the FR and the HH beams analytically.

Let the real part of the refractive index of the surrounding medium be n_1 (typically vacuum) and of the wedge material n_2. Then, Brewster's angle for the p-polarized fundamental beam is given by:

$$\phi_B = \arctan \frac{n_2}{n_1}. \tag{1}$$

The HH radiation will be reflected by the WOMOC under this angle. By Snell's law, the refraction angle for the beam transmitted through the $n_1 - n_2-$interface equals:

$$\phi'_B = \arcsin\left(\frac{n_1}{n_2} \cdot \sin\phi_B\right). \tag{2}$$

The incidence angle ϕ_i of the fundamental beam on the subsequent layer is:

$$\phi_i = \phi'_B + \alpha. \tag{3}$$

Figure 1 shows that the outgoing angle ϕ_j of the reflected fundamental beam is:

$$\phi_j = \phi'_B + 2\alpha. \tag{4}$$

#146865 - $15.00 USD Received 29 Apr 2011; revised 30 May 2011; accepted 30 May 2011; published 7 Jun 2011

Applying Snell's law again we obtain the following output angle of the fundamental beam with respect to the WOMOC surface normal:

$$\beta = \arcsin\left(\frac{n_2}{n_1}\cdot\sin\phi_j\right) \tag{5}$$

$$= \arcsin\left\{\frac{n_2}{n_1}\cdot\sin\left[\arcsin\left(\frac{n_2}{n_1}\cdot\sin(\arctan\frac{n_2}{n_1})\right)+2\alpha\right]\right\}. \tag{6}$$

Now we can compute the separation angle between the HH beam and the FR beam upon reflection at the WOMOC:

$$\delta = \beta - \phi_B. \tag{7}$$

Because the wedge layer is very thin, we can assume for simplicity that both the HH and the FR beams leave the WOMOC at the same position, with an angle δ between them. After a propagation distance L the spatial separation d between the centers of the two beams equals:

$$d = L\cdot\tan(\delta). \tag{8}$$

The reflection power losses R_{loss} of the FR at the WOMOC owed to the deviation from Brewster's angle when the beam exits the wedge, assuming a collimated beam, can be calculated by means of the Fresnel equations and are given by the following expression:

$$R_{loss} = \left|\frac{n_2\sqrt{1-\left(\frac{n_2}{n_1}\sin\phi_j\right)^2}-n_1\cos\phi_j}{n_2\sqrt{1-\left(\frac{n_2}{n_1}\sin\phi_j\right)^2}+n_1\cos\phi_j}\right|^2. \tag{9}$$

Note that here we have chosen Brewster's angle as the angle of incidence of the incoming beam for the simplicity of the derivation. In fact, choosing a slightly different angle of incidence can even decrease the FR reflection losses while the beam separation angle δ stays nearly constant. The special cases in which (i) the incident beam (FR+HH) strikes the WOMOC surface under Brewster's angle (i.e. the case discussed here) and (ii) the FR beam leaving the wedge exits under Brewster's angle exhibit two particularities, which might be desirable: in case (i) the residual FR co-propagating with the HH beam upon reflection at the WOMOC is minimized. In case (ii), the residual FR propagating inside the wedge is minimized.

3.2. A quantitative example

As a quantitative example, we consider SiO_2 (fused silica) as the material of the wedge, with the refractive index $n_2 = 1.47$ for the FR (optical dispersion is neglected in this example). With $n_1 = 1$ we obtain the Brewster angle $\phi_B = 55.77°$. Figure 2 shows the separation angle δ as well as the losses R_{loss} as functions of the wedge angle α. The wedge-induced loss R_{loss} limits the theoretically achievable power enhancement in an enhancement cavity containing this element to $1/R_{loss}$ (see e.g. [4] for details). The XUV reflectivity at 60 nm amounts to ∼10% [21].

Figure 3 shows the region around the focus of a standard-design bow-tie enhancement cavity for HHG, with an implemented WOMOC. Note that for visualization purposes, the figure is not to scale. In this example, we consider a 78 MHz repetition rate infrared FR cavity, similar to the one presented in [9]. However, in contrast to [9], asymmetric focusing is used to increase the distance from the cavity focus to the subsequent curved mirror, facilitating the inclusion of the WOMOC. The radii of curvature of the spherical mirrors C_1 and C_2 are 100 and 200 mm, respectively. In the cavity stability range center this results in a focus radius of 22 μm. The WOMOC is placed 50 mm after the focus. The FR beam radii ($1/e^2$ of the intensity) at mirror

#146865 - $15.00 USD Received 29 Apr 2011; revised 30 May 2011; accepted 30 May 2011; published 7 Jun 2011

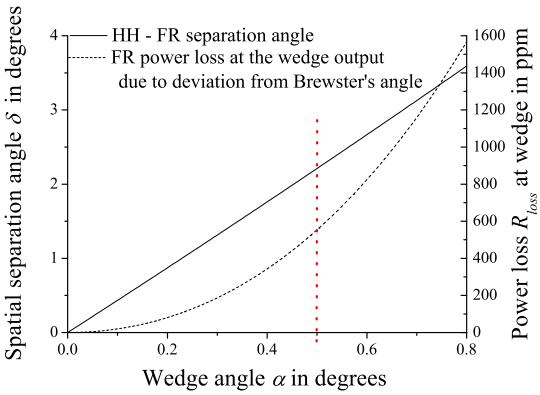

Fig. 2. Spatial separation angle δ between the FR and the HH upon reflection at the WOMOC and FR losses R_{loss} at the exit of the wedge due to deviation from Brewster's angle as functions of the wedge angle α for the wedge material SiO_2 (refractive index=1.47). The dotted line (red) indicates the values for the prototype presented in Section 4.

C_1, at the WOMOC and at mirror C_2 are 0.7, 0.7 and 1.6 mm, respectively. The incidence angle on the WOMOC surface corresponds to the Brewster angle ϕ_B. We choose a wedge angle $\alpha = 0.5^\circ$, leading to a separation angle $\delta = 2.2^\circ$ between the XUV and the FR. On the one hand, this small wedge angle enables the realization of a thin wedge layer, implying low losses and nonlinearities. On the other hand, after propagating 50 mm from the WOMOC to mirror C_2, the centers of the two beams are $\sim$2 mm apart, making the XUV output coupling possible. The theoretical losses R_{loss} amount to 554 ppm, allowing for a power enhancement exceeding 1800.

In order to increase the distance from the WOMOC to the next mirror for a certain wedge angle and, thus, increase the spatial separation of the FR and HH at the position of this mirror, additional curved mirrors can be implemented in the cavity. Alternatively, the curved mirror after the HHG focus could be placed under oblique incidence, as can be done e.g. with parabolic mirrors. This mirror could on the one hand nearly collimate the FR beam and on the other hand reflect a substantial portion of the generated XUV due to the large angle of incidence. Placing a WOMOC after this mirror could therefore bare several advantages over placing it between the focus and this mirror. Firstly, the FR is (nearly) collimated, implying Brewster angle incidence over the entire beam profile. Secondly, the spatial constraint imposed to the separation angle δ, and, therefore to the wedge angle α by the mirror following the WOMOC can be relaxed if the mirror following the WOMOC is placed at a large distance.

3.3. Advantages of the WOMOC

While the spatial separation of the FR and the HH at the surface of the WOMOC relies on the same physical principle as in the case of the free-standing Brewster plate output coupler and the output coupling efficiencies of both methods are identical, the WOMOC exhibits several advantages which are discussed in the following.

The WOMOC is a robust, compact optical element enabling easy handling and processing in contrast to free-standing foils/plates. This allows for the production of a very thin wedged layer, introducing low additional absorption, heat production and other losses to the FR. A particular advantage of the small material thickness is the reduction of dispersion and nonlinear effects. These properties are particularly valuable in the case of resonant cavities. Furthermore, it facilitates good control of the optical quality of the surface, even for a very thin wedged

#146865 - $15.00 USD Received 29 Apr 2011; revised 30 May 2011; accepted 30 May 2011; published 7 Jun 2011

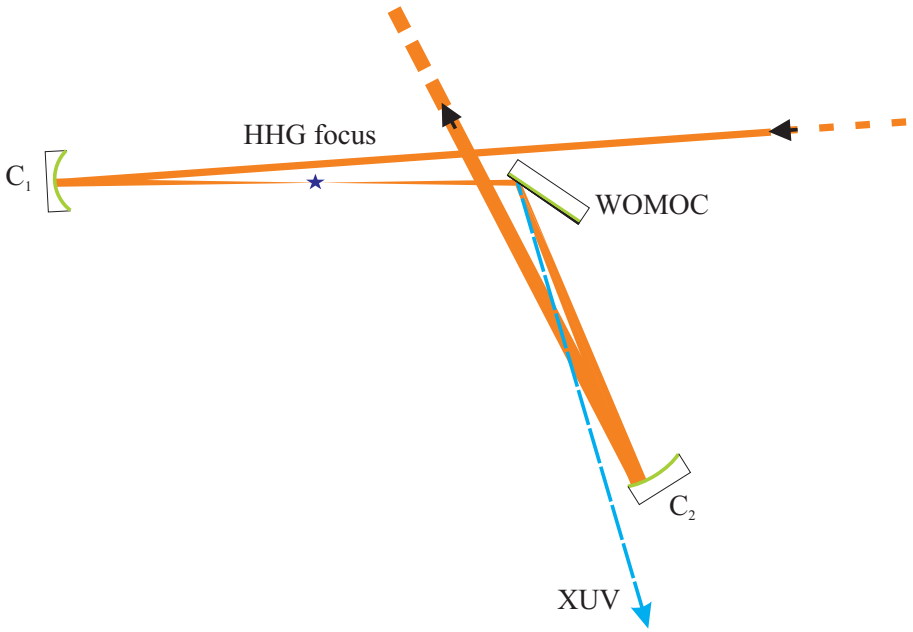

Fig. 3. WOMOC implementation in a standard-design bow-tie ring cavity. Mirrors C_1 and C_2 are the curved mirrors with radii of curvature equal to 100 and 200 mm, respectively. All other cavity mirrors can be plane mirrors and are left out here for simplicity. High harmonics are generated collinearly with the laser in the focus.

layer. Also, this robust element is easier to align, to handle and to mount and mechanically more stable than a free-standing thin plate.

One surface of the wedged layer, through which the FR passes, is attached to a large optical element, enabling the efficient transport of heat generated by the absorption in the wedge material, away from the illuminated area. A thorough investigation of the heat conduction properties exceeds the scope of this paper. However, the experimental results presented in the subsequent section illustrate the improved heat conduction. Recent experimental results in our group indicate that thermal effects in the free-standing Brewster plate represent the current limitation of power scaling in an enhancement cavity including such an output coupler. Thus, the increased efficiency of the heat transport is expected to boost the achievable intracavity power levels.

While the FR passes through the wedge, it accumulates group delay dispersion. Knowing the material and geometric properties of the wedge, this dispersion can be estimated and compensated by the mirror coating design. By a slight transverse translation of the WOMOC, the length of the FR beam path inside the wedge can be varied, such that the incidence angles are not affected. In this manner, a fine tuning of the FR dispersion upon reflection at the WOMOC can be achieved. The significance of this property increases with shorter pulses. For the determination of the dispersion during this fine tuning process, the method presented in [13] can be employed. Furthermore, both the wedged upper layer and the Brewster angle incidence represent advantages from the point of view of the low-dispersion design criterion, see [22] and [23], respectively.

#146865 - $15.00 USD Received 29 Apr 2011; revised 30 May 2011; accepted 30 May 2011; published 7 Jun 2011

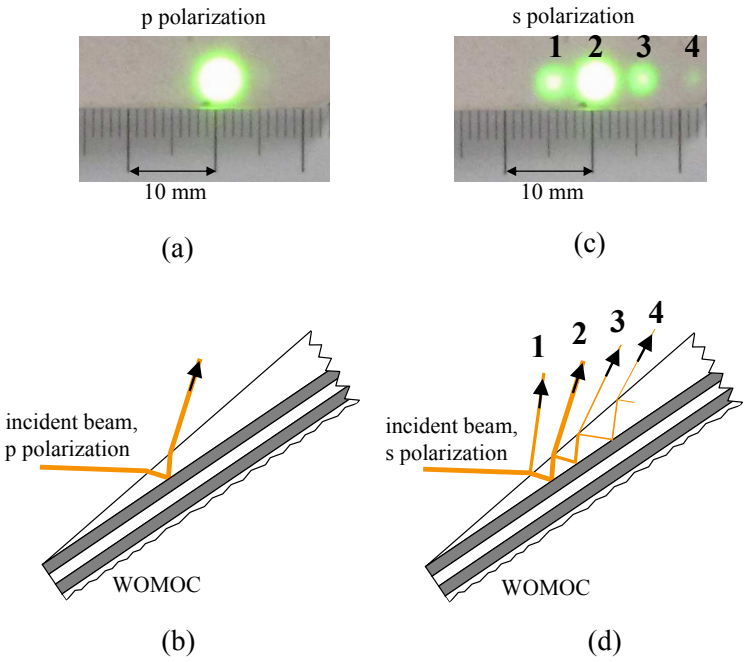

Fig. 4. Experimental demonstration of the spatial separation property of the WOMOC: reflection of a beam impinging under Brewster's angle on the surface of the WOMOC, after a propagation of 100 mm. (a) and (b): visualization of the beam with an IR-sensitive card and sketch of beam propagation path in the WOMOC, respectively, for p-polarized light. (c) and (d): s-polarized light. Spot 1: direct reflection from the wedge surface, spot 2 beam penetrating the wedge and reflected at the multilayer, spots 3 and 4 are cause by multiple reflections inside the wedge.

4. Experimental results

4.1. Technical realization

To demonstrate the technical feasibility of the WOMOC we produced a prototype according to the example considered in Section 3.2. Firstly, a standard low-loss dielectric quarter-wave stack coating for the highly reflective mirror underlying the wedged top layer was designed. The reflectivity was maximized for the central wavelength of 1040 nm and the coating design was matched to the refractive index of the wedge material, i.e. $n_2 = 1.47$ and to the inner angle of incidence of $\phi_i = 34.2^\circ$. This coating was ion-beam sputtered onto a standard 1-inch-diameter fused silica substrate. Secondly, a 0.5 mm fused silica plate with parallel surfaces was optically contacted to the surface of the coated mirror. Thirdly, to obtain the wedge and optimum optical quality of the surface, the top layer was lapped and polished under an angle $\alpha = 0.5^\circ$ over the entire surface. The small wedge angle implies a short propagation length through the wedge material. Therefore, no further dispersion compensation was accounted for in the coating design.

#146865 - $15.00 USD Received 29 Apr 2011; revised 30 May 2011; accepted 30 May 2011; published 7 Jun 2011

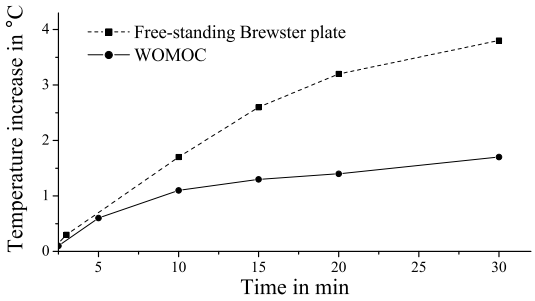

Fig. 5. Comparison of the evolution of the temperature increase from room temperature measured at the surface of a free-standing Brewster plate and the surface of the WOMOC. Both were illuminated with a 40-W beam under Brewster's angle in a vacuum chamber.

4.2. Characterization

In a first experiment, we tested the spatial separation property of the prototype. The linearly polarized output beam of our seeding laser [24] with a central wavelength of 1040 nm and with an average power of 0.5 W is sent to the surface of the WOMOC under $\phi_B = 55.8^\circ$ angle of incidence. Figure 4 shows the beam path as well as the laser spots detected with an IR-sensitive card after propagating 100 mm away from the WOMOC surface, for p and for s polarization. For p polarization we observe a single reflection, see Figs. 4(a) and 4(b). In order to detect the direct reflection from the wedge surface, we rotated the polarization of the incident beam by 90 degrees with a half-wave plate. We observe several spots, see Figs. 4(c) and 4(d). The spot numbered by 1 is caused by direct reflection from the wedge surface. Spot 2 stems from the portion of the beam which penetrates the wedge layer, is reflected by the multilayer coating and exits the wedge. Before exiting the wedge, a portion of this beam is reflected back into the wedge layer at the wedge-air interface. Subsequently, this portion is again reflected by the multilayer and is split into the beam leading to spot 3 and into another back reflection from the wedge-air interface. This reflection pattern is repeated and gives rise to spot 4. On the right-hand side of spot 4, further spots with decreasing intensities can be detected (not shown here). A collinear combination of a p-polarized VIS/IR beam and its HH, incident under $\phi_B = 55.8^\circ$ on the WOMOC surface would be split into a single reflection of the FR, indicated by the single spot in Fig. 4(a) and located at the position of spot 2 in Fig. 4(c) and into the XUV beam, located at the position of spot 1. The distance between the centers of the two spots is $\sim$4 mm, which is in excellent agreement with the example discussed in Section 3.2.

To determine the reflection losses for the p-polarized FR impinging on the WOMOC surface under $\phi_B = 55.8^\circ$, we performed a standard ring-down measurement. Over the entire bandwidth of our seeding laser, losses in the range 500-600 ppm were measured, which is in excellent agreement with the value calculated in Section 3.2, see Fig. 2.

The last experiment illustrates the heat conduction improvement of the WOMOC compared to a free-standing Brewster plate, with a comparable thickness. The WOMOC and a 100 μm thin fused silica plate (same material as the wedge layer of the WOMOC) were illuminated with 40 W average power. Both elements were mounted at Brewster's angle in a vacuum chamber. The collimated beam was p-polarized and had a radius of 1.8 mm. The light transmitted through and reflected by the Brewster plate and the WOMOC, respectively, was steered out of the chamber to avoid residual heating. The pressure in the vacuum chamber was $< 10^{-1}$ mbar. With an IR thermometer (Voltcraft IR-1001A) the temperature of the surface of the optical el-

#146865 - $15.00 USD Received 29 Apr 2011; revised 30 May 2011; accepted 30 May 2011; published 7 Jun 2011

ements was measured through a zinc selenide vacuum chamber window, which is transparent for mid-infrared heat radiation. The Brewster plate was mounted by clamping its lower edge mechanically and the WOMOC was mounted in a standard mirror mount. Figure 5 shows the temperature increase from room temperature measured over a time of 30 minutes and clearly indicates that the WOMOC exhibits superior heat conduction. In the case of a high-power application, such as XUV output coupling from an enhancement cavity, with average powers in the multi-kW range, this advantage is expected to play a decisive role. It should also be mentioned that the heat transport away from the illuminated spot can be improved for both optical elements by means of their mounting. A detailed analysis of the heat transport mechanisms and an optimization of the mechanical mounts exceeds the scope of this paper such that the results plotted in Fig. 5 should be interpreted qualitatively rather than quantitatively.

5. Conclusion

The concept, realization and experimental characterization of a novel low-loss VIS/IR-XUV beam splitter, suitable for high-power applications, is presented. The spatial separation of the XUV from the VIS/IR spectral components is achieved by the wedged top layer of a dielectric multilayer structure and relies on the same physical mechanism as in the case of a free-standing Brewster plate. However, the robustness of our beam splitter leads to two advantages over a free-standing thin Brewster plate. On the one hand, the heat conduction is significantly improved, allowing for operation at higher powers. On the other hand, mechanical handling becomes easier. In particular, this allows for high-optical-quality fabrication, even for an extremely thin top layer. We demonstrate experimentally the spatial separation, the high reflectivity for the fundamental radiation as well as the improved heat conduction. With a fused silica wedge with an angle of only 0.5° we achieve a spatial separation angle of 2.2°, which is enough to couple out high harmonics from a standard-design enhancement cavity. The measured reflectivity for the fundamental radiation is 0.9995. The reflectivity in the XUV spectral region is subject to further investigation. However, since a better optical quality is achievable due to the element's robustness, the XUV reflectivity is expected to surpass the value of a free-standing Brewster plate from the same material as the wedge layer.

The beam splitter was primarily designed as a *wedge-on-mirror output coupler* (WOMOC) for collinear output coupling of intracavity-generated high-harmonic radiation, circumventing limitations of current methods. It is expected to enable a significant boost of the power regime in intracavity HHG experiments in the near future. In addition, the WOMOC might also be employed to separate the XUV from the FR in single-pass HHG systems or to combine a VIS/IR and an XUV beam collinearly, e.g. for pump-probe experiments.

Acknowledgments

The prototype was fabricated by the company Layertec GmbH. The authors gratefully acknowledge the support of Dr. Peter Zimmermann from Layertec and wish to thank their colleagues: Jan Kaster for preparing the vacuum chamber for the heat measurement experiment, Vladimir Pervak, Oleg Pronin and Alexander Apolonski for helpful discussions. This work was supported by the Deutsche Forschungsgemeinschaft (DFG) Cluster of Excellence, Munich Centre for Advanced Photonics (MAP) (www.munichphotonics.de) and by the BMBF via PhoNa (Photonische Nanomaterialien).

#146865 - $15.00 USD Received 29 Apr 2011; revised 30 May 2011; accepted 30 May 2011; published 7 Jun 2011